Modal truncation issues in synthesis procedures for vibratory power flow and dissipation

Todd E. Rook[a] and Rajendra Singh[b]

Acoustics and Dynamics Laboratory, Department of Mechanical Engineering, The Ohio State University, Columbus, Ohio 43210-1107

(Received 14 February 1995; accepted 12 December 1995)

Truncation of component modes in synthesis techniques may cause significant errors in the calculation of localized harmonic vibration responses and power flows. Two alternate approaches are proposed to reduce the effects of such errors, and the third approach which combines both with mixed analytical orthonormal bases has been found to be most successful. These concepts are integrated in mobility and modal methods of computing accelerances, input power, transmitted power, and modal dissipation efficiency spectra. Two example cases, namely, the T-beam and a plate–beam structure, are utilized for comparative evaluation of truncation effects. Limited experimental results verify the proposed calculation procedure. © *1996 Acoustical Society of America.*

PACS numbers: 43.40.At, 43.20.Ks

INTRODUCTION

Modal truncation has received much attention in the literature since it affects the calculation of natural frequencies and dynamic displacement of an assembled structure or equipment.[1–8] Several component mode synthesis methods such as inertia relief, attachment or constrained modes,[3–5] and mode acceleration methods[6,7] have been employed to improve the static completeness of the modal bases. Two fundamental issues, however, remain unresolved. First, truncation of component modes in modal synthesis techniques poses many difficulties, especially for complicated structures. Different linearly independent bases such as Lanczos vectors[9–12] and component modes with various interface conditions[13] have been proposed to improve the completeness and convergence of modal superposition. Second, serious computational problems may arise when localized dynamic responses and mechanical power flow, say, near stress concentrations,[14] boundaries, junctions, or excitations, are of interest. For example, Gavric and Pavic[15,16] have reported difficulties in the case of structural intensity calculations based on a finite element method for both global and local properties. If a component mode synthesis technique is utilized to calculate both natural frequencies and dynamic power, both of the above-mentioned issues compound the computational considerations. In layman's terms, it might be viewed as "double jeopardy." Such particular difficulties associated with implementing power flow calculations within a synthesis procedure were demonstrated in a recent article by Farstad and Singh[17] which also presents a detailed review of the state of art. Before proceeding further, it is worth mentioning that there is a significant body of literature on dynamic condensation and lumping schemes such as Guyan reduction,[18] substructuring, and superelements[19] which reduce the spatial dimension of a discrete system to a more tractable size while retaining sufficient dynamics such as modes retained in order to primarily economize the eigenvalue computations.

The focus of this paper is on the computation of vibratory power flow and dissipation on a narrow-band basis at lower frequencies when specific assembly modes may be excited by sinusoidal or periodic disturbances. Power flow synthesis-type methods are very appealing because of the flexibility of analyzing each component separately and the inherent design implications in terms of both modal solutions and damping treatments; see Refs. 17 and 20 for more discussion. Related literature, except for three recent articles,[15–17] does not seem to address the effect of modal truncation on the vibratory power flow even though eigenvalue issues have been discussed in depth.[1–13] Two relevant articles[15,16] use a swept static solution that purges the contributions of retained modes in static response and thereby maintain the static completeness. The third paper[17] uses constrained interface modes to improve convergence, though static completeness is not ensured. The current article extends the recent study on straight beams with rigid joints by Farstad and Singh[17] but a different mathematical framework with emphasis on compliant joints and more complicated examples have been chosen which are described in the next section.

I. PROBLEM FORMULATION

Figure 1 illustrates the conceptual source(s)–path(p)–receiver(c) model of the linear discrete dynamic system. This representation is especially attractive from the viewpoint of analyzing paths (b) and mechanical connections for reduced vibroacoustic response. The multidimensional compliant joints are considered massless, and are therefore only characterized by their stiffness, $\mathbf{K}_p$, and damping, $\mathbf{C}_p$, matrices which are of dimension $2N_p$, and are assumed symmetric for the sake of convenience. The dimensions of source and receiver are characterized by N_s and N_c, respectively,

[a]Currently with the Copeland Corporation, Sidney, Ohio.
[b]Corresponding author: Phone (614) 292-9044; Fax (614) 292-3163.

 0001-4966/96/99(4)/2158/9/$6.00

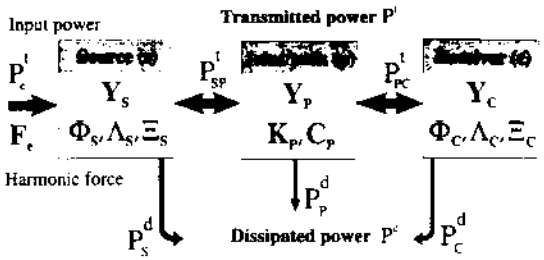

FIG. 1. Schematic of source–path–receiver model.

each of which also includes the path dimension N_p. Hence, the overall system dimension is $N_z = N_s + N_c$.

In a recent paper[20] we presented two different power flow synthesis methods which are conceptually illustrated in Fig. 1. In both of these methods, the transmitted or dissipated power was expressed[20] as a quadratic form of the excitation

$$P(\omega) = \mathbf{F}_e^H(\omega)\mathbf{Q}(\omega)\mathbf{F}_e(\omega), \tag{1}$$

where $\mathbf{Q}$ is a matrix containing either mobility matrices or modal matrices. Since the mobility matrices themselves are derived from modal expansions,[20,21] it is apparent that the power flows predicted by either method depend heavily on the modal bases and hence are sensitive to truncation. To examine it further, recognize that for the untruncated basis the system dimension is N_z which includes N_s modes of the source and N_c modes of the receiver. In our approach we truncate the constrained source component to n_s where $n_s < N_s$ and the constrained receiver to n_c where $n_c < N_c$. The resulting dimension of the system is now $n_z = n_s + n_c + 2N_p$ where $n_z < N_z$. Unlike the analogous previous definition of the untruncated dimension $N_z = N_s + N_c$, the truncated dimension n_z has the addition of the $2N_p$ term due to the fact that n_s and n_c refer to the constrained components with fixed interface degrees of freedom which must each be augmented with the interface degrees of freedom N_p. This information can be mapped in terms of frequencies. Assume the frequency range of interest for the assembled system is from 0 to ω_h. Natural frequencies of the highest n_s and n_c modes retained in the source and receiver components are $\omega_s^{n_s}$ and $\omega_c^{n_c}$, respectively; note that $\omega_s^{n_s}$ and $\omega_c^{n_c}$ may not be equal. Here, modes and natural frequencies refer to those of the component subject to constraints at the interface. These modes are used in the subsequent discussions and approaches because they approximate the loaded interface conditions[13] that will be realized in the assembly. From the Rayleigh–Ritz method, it is clear that each component is constrained now because of the truncated basis,[13,20] and as a consequence the natural frequencies of the assembly will be overestimated.[22] Three possibilities exist when the highest natural frequency of any component ($\omega_m^{n_m}$; $m = s, c$) that is retained in the analysis is compared with the maximum frequency of interest (ω_h) for the assembly:[23–25]

(1) $\omega_m^{n_m} \ll \omega_h$: This case is of academic interest since it will not provide a sufficient basis.

(2) $\omega_m^{n_m} \geqslant \omega_h$: The truncation effect for power flow quantities may be similar to those observed in the calculation

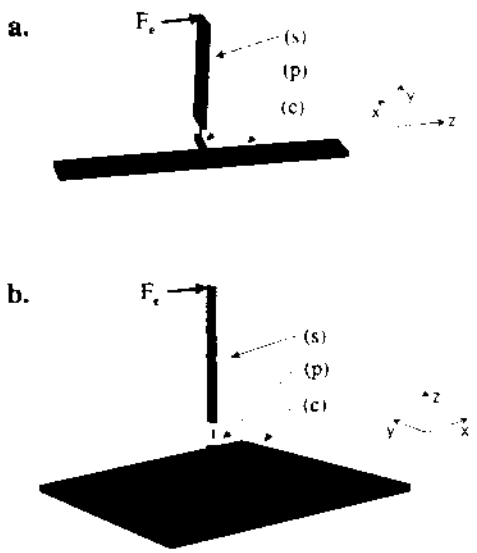

FIG. 2. Example cases. (a) T-beam, (b) plate–beam structure.

of assembly natural frequencies and dynamic displacements provided the residual modal terms are negligible.

(3) $\omega_m^{n_m} \gg \omega_h$: This case appears to be more realistic for power flow calculations than case 2 as demonstrated by Farstad and Singh[17] for the fixed–fixed beam example. For practical purposes, we assume that $\vartheta(\omega_m^{n_m}) = \vartheta(10\omega_h)$ when $\vartheta(\,)$ is the order of magnitude.

In order to quantify how modal truncation affects the synthesis methods,[20] two example cases will be utilized. First a T-beam structure as shown in Fig. 2(a) is selected due to its wide acceptance as a paradigm for power flow studies.[26–32] Although the structure is geometrically quite simple, it exhibits the necessary characteristics we wish to study, such as vector transmission paths (i.e., vector and moment paths). The simplicity of this structure also permits both analytical and experimental studies to be conducted. The physical structure consists of two steel beams welded together, one (the source) 254 mm in length with the other (the receiver) twice that length. Both are 3.175 mm thick and 25.4 mm wide. Analytically, the T-beam is modeled by writing a finite element (FEM) code based on two-node Timoshenko beam elements[33] with nodal DOF $\mathbf{q}(t) = \{u_y, \theta_x, u_z\}^T$. For the lower frequency range, in which we are interested, this 1-D modeling will be adequate. Additionally, the joint is modeled as a short beam element at the interfaces of the two.

The second example case is similar to the T-beam but more complex in the sense that it involves the junction between a beam with flexure in two planes and an elastic plate; see Fig. 2(b). Similar structures have appeared in the literature for broadband power flow studies, though with different joints[34] and boundary conditions.[35] The experimental fixture consists of a 12.7-mm^2 aluminum beam which is 304.8 mm long, bolted to a 127 mm×228.6 mm aluminum plate which is 6.35 mm thick. For our analysis of the structure, it is modeled by 2-D Timoshenko beam elements[33] and four noded plate elements with flexural and in-plane degrees of freedom[33,36] such that the nodal displacements are

$\mathbf{q}(t)=\{u_z, \theta_x, \theta_y, u_x, u_y\}^T$. As before, the joint is modeled as a small beam element at the interface of the two substructures. Experimental studies for either example case are limited to the measurement of natural frequencies and frequency response curves (in terms of accelerance or mobility) of the assembly, which are primarily employed to validate theory. Then transmitted and dissipated powers are calculated. Three analytical approaches are proposed to specifically address the effects of truncated component modes.

II. APPROACH A: TRUNCATION OF CONSTRAINED INTERFACE COMPONENT EIGENVECTORS

Since many of the problems of modal truncation are somehow related to the particular choice of orthonormal bases used to characterize the components, we will first investigate the effects of different bases on the proposed power flow methods. In this section, the component bases will consist of the component eigenvectors with fixed (constrained) boundary conditions imposed at the interfaces. This basis (subsequently abbreviated as CE for constrained eigenvectors) is in direct contrast to the free (or unconstrained) interface eigenvectors (similarly referred to as UE) of the previous article.[20] A detailed procedure to obtain the component bases and to then augment its static completeness will be presented next. It should be noted that the power flow procedures of this and the previous article[20] assume that a discretized basis exists (such as from FEM), and furthermore the procedures of this article require that discretized mass and stiffness matrices are available. Since continuous bases are available only for very simple structural geometries with classical boundary conditions, the use of discretized bases for practical systems is obviously not a liability. The reader is well advised to read Ref. 20 before proceeding further.

The first step is to partition the component matrices into interface (b) and interior (i) degrees of freedom (DOF). For example, the stiffness matrix ($\mathbf{K}$) of the source component (s) would become

$$\mathbf{K}_s=\begin{bmatrix} \mathbf{K}_s^{bb} & \mathbf{K}_s^{bi} \\ (\mathbf{K}_s^{bi})^T & \mathbf{K}_s^{ii} \end{bmatrix}. \tag{2}$$

At this stage, it may be desirable to perform an initial Guyan reduction[18] of the interior DOF in order to reduce the dimension of the problem while maintaining static completeness of the bases (implicit in the system matrices). Then the component matrices will be modified as follows where i' denotes the retained interior DOF, commonly referred to as the master DOF:[18]

$$\mathbf{K}_s'=\begin{bmatrix} \mathbf{K}_s^{bb} & \mathbf{K}_s^{bi'} \\ (\mathbf{K}_s^{bi'})^T & \mathbf{K}_s^{i'i'} \end{bmatrix}. \tag{3}$$

The second step is to create a transformation matrix for each component. The goal is to ensure that modal bases corresponding to he transformed component mass and stiffness matrices will converge quickly. An example of a transformation matrix[17] for the source is obtained by also partitioning the displacement vector, $\mathbf{u}$ as follows:

$$\begin{Bmatrix} \mathbf{u}_s^b \\ \mathbf{u}_s^{i'} \end{Bmatrix}=\begin{bmatrix} \mathbf{I} & \mathbf{0} \\ \mathbf{A}_s^b & \mathbf{\Psi}_s^{ce} \end{bmatrix}\begin{Bmatrix} \mathbf{u}_s^b \\ \boldsymbol{\eta}_s^{i'} \end{Bmatrix}. \tag{4a}$$

$$\mathbf{\Gamma}_s=\begin{bmatrix} \mathbf{I} & \mathbf{0} \\ \mathbf{A}_s^b & \mathbf{\Psi}_s^{ce} \end{bmatrix}\equiv N_s\times N_s', \tag{4b}$$

where the reduced source component dimension is $N_s' = N_s^b + N_s^{i'}$ and $\mathbf{A}_s^b = -(\mathbf{K}_s^{i'i'})^{-1}\mathbf{K}_s^{i'b}$ may be considered the static influence (Green's function) matrix,[17] which represents the interior displacement responses due to unit displacements at the interface. Furthermore, $\mathbf{\Psi}_s^{ce}$ represents the interior eigenvectors subject to constrained boundary conditions at the interfaces. The issue of truncation arises here in the determination of how many modes to retain in $\mathbf{\Psi}_s^{ce}$; truncating any mode obviously destroys the static completeness which has been maintained until this stage. Therefore, if only the modes of $\mathbf{\Psi}_s^{ce}$ which lie in the frequency range of interest are retained, the basis must be augmented to account for residual effects. Many methods[3–7] exist to improve the basis, but in this paper a method similar to mode acceleration methods[6,7] and higher-order modal methods[37–39] is utilized. In this case the transformation matrix becomes

$$\begin{Bmatrix} \mathbf{u}_s^b \\ \mathbf{u}_s^{i'} \end{Bmatrix}=\begin{bmatrix} \mathbf{I} & \mathbf{0} & \mathbf{0} & \mathbf{0} \\ \mathbf{A}_s^b & \mathbf{\Psi}_s^{ce} & \mathbf{B}_s^b & \mathbf{C}_s^b \end{bmatrix}\begin{Bmatrix} \mathbf{u}_s^b \\ \boldsymbol{\eta}_s^{i'} \\ \ddot{\mathbf{u}}_s^b \\ \dddot{\mathbf{u}}_s^b \end{Bmatrix}, \tag{5a}$$

$$\mathbf{\Gamma}_s=\begin{bmatrix} \mathbf{I} & \mathbf{0} & \mathbf{0} & \mathbf{0} \\ \mathbf{A}_s^b & \mathbf{\Psi}_s^{ce} & \mathbf{B}_s^b & \mathbf{C}_s^b \end{bmatrix}\equiv N_s\times(n_s+3\cdot N_s^b), \tag{5b}$$

$$\mathbf{A}_s^b=-(\mathbf{K}_s^r)^{-1}\mathbf{K}_s^{i'b}, \tag{5c}$$

$$(\mathbf{K}_s^r)^{-1}=(\mathbf{K}_s^{i'i'})^{-1}-\mathbf{\Psi}_s^{ce}(\mathbf{\Lambda}_s^{ce})^{-1}(\mathbf{\Psi}_s^{ce})^T, \tag{5d}$$

$$\mathbf{B}_s^b=(\mathbf{K}_s^{i'i'})^{-1}\mathbf{M}_s^{i'i'}\mathbf{A}_s^b-(\mathbf{K}_s^r)^{-1}\mathbf{M}_s^{i'b}, \tag{5e}$$

$$\mathbf{C}_s^b=-(\mathbf{K}_s^{i'i'})^{-1}\mathbf{M}_s^{i'i'}\mathbf{B}_s^b, \tag{5f}$$

where the dimension of the transformation matrix is $n_s+3\cdot N_s^b$ where $n_s<N_s$ and $\mathbf{A}_s^b$,$\mathbf{B}_s^b$, and $\mathbf{C}_s^b$ are the first-, second-, and third-order correction terms, respectively.[37] Here $\mathbf{A}_s^b$ is the static influence (Green's function) matrix as modified by the mode acceleration method[6] to contain the residual flexibility $(\mathbf{K}_s^r)^{-1}$. In the above equation $\mathbf{\Psi}_s^{ce}$ and $\mathbf{\Lambda}_s^{ce}$ refer to the retained modes and eigenvalues of the constrained interior problem (consequently there are no zero eigenvalues and the matrix $\mathbf{\Lambda}_s^{ce}$ is invertible). Also from above one may see why it was stipulated that an access to the mass stiffness matrices is needed for this method. The transformation matrix may be rewritten as

$$\mathbf{\Gamma}_s=\begin{bmatrix} \mathbf{I} & \mathbf{0} \\ \mathbf{A}_s^b & \mathbf{\Theta}_s \end{bmatrix}, \tag{6a}$$

$$\mathbf{\Theta}_s=[\mathbf{\Psi}_s^{ce} \quad \mathbf{B}_s^b \quad \mathbf{C}_s^b]. \tag{6b}$$

From this form, it is apparent that the columns of $\mathbf{\Theta}_s$ must be linearly independent if the positive definiteness of the mass matrix is to be preserved. Therefore the columns of $\mathbf{\Theta}_s$ may require reorthogonalization via a Gram–Schmit technique.

However, since the columns of Ψ_s^{ce} are already orthogonal, computational effort may be saved by only reorthogonalizing the columns of $\mathbf{B}_s^b$ and $\mathbf{C}_s^b$ with the last column of Ψ_s^{ce}. Recall that this whole step must be done for each component (source and receiver).

The final three steps involve (i) transforming the component mass and stiffness matrices, (ii) performing the eigenanalysis of these transformed component matrices, and (iii) calculating powers P^t and P^d by using the synthesis procedure (either modal or mobility method). For example, the transformed source component matrices are given by $(\mathbf{\Gamma}_s)^T\mathbf{K}_s'\mathbf{\Gamma}_s$ and $(\mathbf{\Gamma}_s)^T\mathbf{M}_s\mathbf{\Gamma}_s$ where both are of dimension $n_s + 3 \cdot N_s^b$. It should be pointed out that no further truncation should be undertaken at this point as it would undermine the efforts of the second step. It should also be noted that the proposed synthesis procedures of the previous paper require only eigenanalyses of the components. Unlike other synthesis procedures,[17] no additional eigenanalysis of the synthesized assembly is necessary thereby resulting in considerable computational savings.

III. APPROACH B: TRUNCATION OF CONSTRAINED INTERFACE COMPONENT LANCZOS VECTORS

In some literature,[9–12] Lanczos vectors have achieved some success in improving the static completeness of bases for dynamic analyses. Consequently they will be utilized in our analysis as an alternative to approach A; this basis will subsequently be referred to as CL for constrained Lanczos vectors. The primary difference between approach A and approach B is in the second step. The transformation matrix given by Eq. (4b) instead contains Ψ_s^{cl} instead of Ψ_s^{ce} where Ψ_s^{cl} now represents the interior Lanczos vectors subject to constrained boundary conditions at the interfaces.[9] In the generating algorithm for Lanczos vectors,[9–12] usually the first Lanczos vector is chosen to be the static displacement of the constrained interior problem. Consequently, in contrast to approach A, truncating the higher vectors does not destroy the static completeness of the basis. Also it has been shown[9] that the Lanczos contains no vectors which are orthogonal to the excitation vector, which is not the case with eigenvectors. Since the Lanczos method automatically discards vectors which do not participate, the CL may be thought of as the minimal basis for the loaded structure. However, as a trade-off, determination of which Lanczos vectors participate in a particular frequency range is not as intuitive as with eigenvectors. Also a trade-off is the fact that, unlike the classical modal (CE) basis, the CL basis is excitation location dependent and thus it must be reformulated for each spatial load distribution. However, since the CL basis does not need to be reformulated at every frequency for a particular excitation, it generally remains quite competitive with the CE basis in terms of its utility in generating frequency response functions. If we choose to augment the basis as in approach A, the transformation matrix of Eq. (5b) remains the same in form except that $\mathbf{A}_s^b$, $\mathbf{B}_s^b$, and $\mathbf{C}_s^b$ are now given by

$$\mathbf{A}_s^b = -(\mathbf{K}_s^r)^{-1}\mathbf{K}_s^{i'b}, \tag{7a}$$

$$(\mathbf{K}_s^r)^{-1} = (\mathbf{K}_s^{i'i'})^{-1} - \Psi_s^{cl}\mathbf{T}_s^{cl}(\Psi_s^{cl})^T, \tag{7b}$$

$$\mathbf{B}_s^b = (\mathbf{K}_s^{i'i'})^{-1}\mathbf{M}_s^{i'i'}\mathbf{A}_s^b - (\mathbf{K}_s^r)^{-1}\mathbf{M}_s^{i'b}, \tag{7c}$$

$$\mathbf{C}_s^b = -(\mathbf{K}_s^{i'i'})^{-1}\mathbf{M}_s^{i'i'}\mathbf{B}_s^b. \tag{7d}$$

Here $\mathbf{A}_s^b$ is again the modified static influence matrix which contains the residual flexibility $(\mathbf{K}_s^r)^{-1}$ but the retained flexibility, $\Psi_s^{cl}\mathbf{T}_s^{cl}(\Psi_s^{cl})^T$, in this expression is different—this has not appeared before in the literature.[9–12] In the above equation Ψ_s^{cl} and $\mathbf{T}_s^{cl}$ refer to the retained Lanczos vectors and a tri-diagonal matrix of scaling factors[10] for the constrained interior problem. It should be pointed out that the attractiveness of the higher-order correction terms ($\mathbf{B}_s^b$ and $\mathbf{C}_s^b$) is that they are calculated much more inexpensively than eigenvectors. However, the computational expenses of those terms and those of Lanczos vectors are of the same order. As a result, when using the transformation of approach B, it seems just as effective to retain more Lanczos vectors rather than augmenting fewer Lanczos vectors with correction terms. Both the correction terms and the Lanczos vectors require the explicit knowledge of the mass and stiffness matrices such as Eqs. (4) and (8) for their generation algorithms.[9–12,37–39]

IV. APPROACH C: TRUNCATION OF MIXED VECTORS

The final approach is simply a combination of approaches A and B. Different types of basis vectors are used for each component, depending on which type best suits them. For our study we propose to employ CL for the source structure and CE for the receiver; other combinations are also possible. Lanczos vectors (CL) are particularly well suited for the source component since they are based on its deflection due to an external load distribution away from the joint interface, and the source is the only component with such a dynamic load applied directly to it. Since the constrained receiver component has no external load associated with it, the CE basis may be most appropriate for it. The CL basis is capable of reproducing the localized responses associated with the source excitation better than the CE basis. Conversely, the CE basis describes the more global excitation-independent response of the receiver well.

V. RESULTS

The T-beam example is used as a vehicle to comparatively evaluate the three approaches. First the synthesis procedure is, however, validated in Fig. 3 by comparing predictions with experimental measurements made on the assembly. The driving point accelerance curves in Fig. 3(a) show a very good match as do the input power spectra in Fig. 3(b), though the experimental measurements of the latter are significantly noisier than that of the former. This is because the normalized input power spectrum is calculated from the quadrature part of the complex-valued accelerance spectrum which has limited dynamic range. These results also show that seven assembly modes lie within our frequency range of interest which has been arbitrarily selected as 0–1600 Hz. This necessitates an absolute minimum of seven assembly DOF—this merely guarantees the existence of seven assembly modes, not that they will match the true modes in this

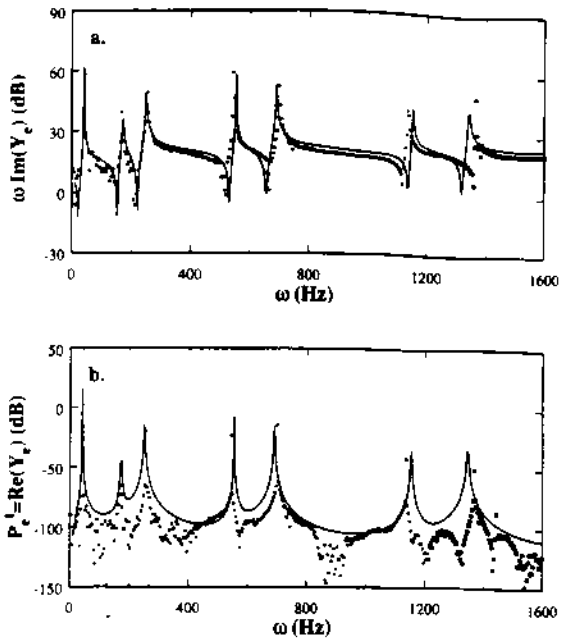

FIG. 3. Validation of power flow synthesis procedure for the T beam of Fig. 2(a). (a) Driving point accelerance, (b) normalized input power. Key: ——— theory, ··· experiment.

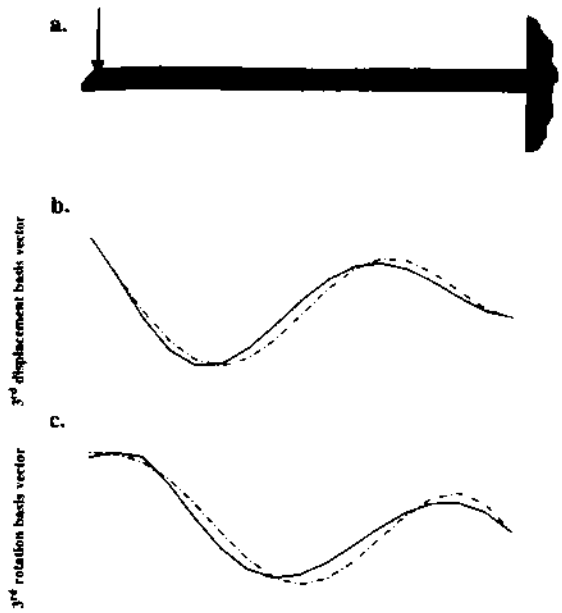

FIG. 4. Comparison of the source component modes for the T beam of Fig. 2(a). (a) Source beam constrained at the interface, (b) transverse displacements of third constrained eigenvector (CE) and constrained Lanczos vector (CL), (c) rotations of third CE and CL. Key: ——— CL, ···· CE.

range. Since we wish to retain as few modes as possible, we will now consider the effect of truncating the bases of the substructures. For the T beam, the synthesis results [with untruncated bases containing 150 DOF and modes of the assembly (N_a) which corresponds to $N_s=51$, $N_c=99$, and $2N_p=6$] of Fig. 3 will be considered the benchmark of our truncation studies. Of interest here are the results when the system dimension is reduced by truncating component modes to n_s and n_c from N_s and N_c, respectively, such that the assembly DOF after truncation is defined as $n_a=n_s+n_c+2N_p$. For the T-beam the following two cases are considered for the sake of illustration (see Table I for more details):

(i) Two (n_s) source CE or CL and four (n_c) receiver CE or CL are retained which yields 12 (n_a) assembly DOF or roughly two times the minimum required DOF, and

(ii) Five (n_s) source CE or CL and ten (n_c) receiver CE or CL are retained which yields 21 (n_a) assembly DOF or three times the minimum required DOF. Figure 4 shows the third CE and CL of the source component, both transverse displacements and rotations, for the sake of comparison. Note that there are pronounced discrepancies in the rotations in the vicinity of the excitation. In Fig. 5(a), approach A is applied without any correction terms. Both of the cases with truncated bases show some discrepancies across the whole frequency range, although the $n_a=21$ case reproduces the resonances more accurately. When the correction terms are added into the bases of approach A [Fig. 5(b)], the accuracy of the $n_a=12$ case increases substantially. When approach B is applied, one may immediately see a better match in Fig. 6(a)—the $n_a=21$ result is nearly identical to the full mode case across the whole frequency range. Furthermore, both the $n_a=21$ and $n_a=12$ cases closely mimic the untruncated case for frequencies up to 400 Hz. A comparison of this to the previous case [Fig. 5(a)] at low frequencies confirms the superior static completeness of approach B over that of approach A. Again the inclusion of correction terms [Fig. 6(b)] improves the synthesized results, particularly for the $n_a=12$ case. The results of using approach C (Fig. 7) are quite similar to those of approach B (Fig. 6), but the $n_a=21$ case with correction terms added [Fig. 7(b)] yields the best match with the benchmark results. The relative strength of approach C is further demonstrated in Fig. 8 when the power transmitted

TABLE I. Dimension and frequencies of truncated components and assembled structure.

	Dimension			Frequencies (kHz)		
Example	n_a	n_s	n_c	ω_h	$\omega_s^{n_s}$	$\omega_c^{n_c}$
T-beam	150	48	96	1.60	179	179
	21	5	10	1.60	2.21	2.21
	12	2	4	1.60	0.244	0.244
Plate–beam	460	50	400	3.20	131	399
structure	45	15	20	3.20	12.5	6.40
	25	5	10	3.20	1.96	1.72

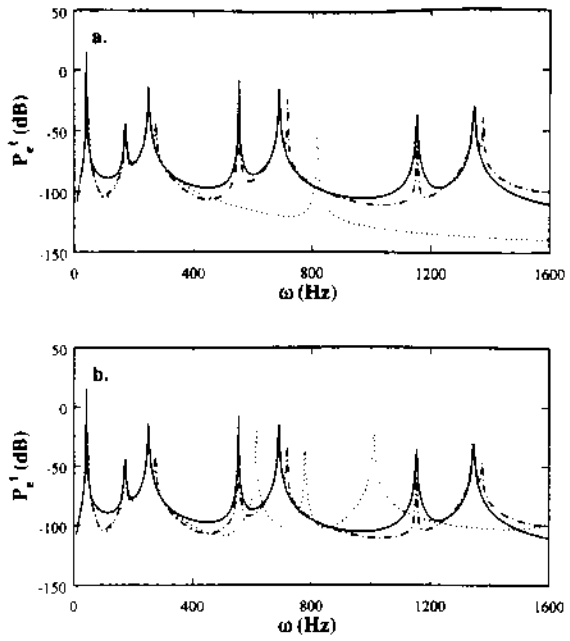

FIG. 5. Effect of modal truncation on normalized input power for the T beam using approach A: (a) without correction terms, (b) with first-order correction terms. Key: ——— n_c=150 (full), ---- n_c=21, ··· n_c=12. Refer to Table I.

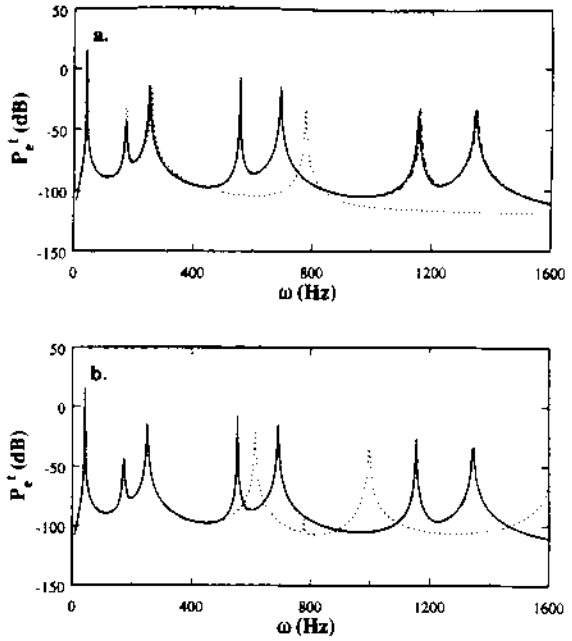

FIG. 7. Effect of modal truncation on normalized input power for the T beam using approach C: (a) without correction terms, (b) with first-order correction terms. Key as in Fig. 5.

through the joint via the force path is calculated. In Fig. 8(a), it is shown that neither the n_c=21 nor n_c=12 cases retain enough dimension to accurately represent longitudinal forces and motions (longitudinal modes are generally higher modes and therefore usually truncated) and thus the power calculations are several orders of magnitude off. However, this deficiency is overcome when correction terms are included as shown in Fig. 8(b). The calculation of power transmitted by moments at the joint shows good matches both with and without correction terms in Fig. 9.

For the plate–beam structure, the synthesis results (with untruncated component bases containing N_s+N_c=460 total DOF and modes which include n_s=50 and n_c=400) of Fig. 10 will be considered the benchmark of our truncation studies. This basis yields a good match with experiment as evi-

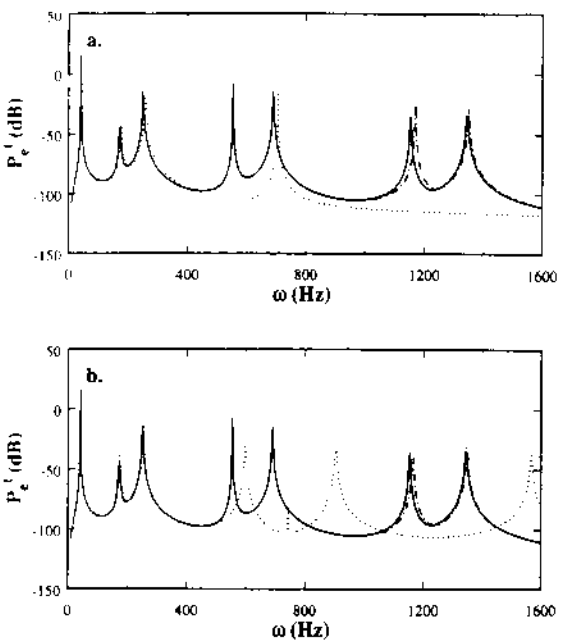

FIG. 6. Effect of modal truncation on normalized input power for the T beam using approach B: (a) without correction terms, (b) with first-order correction terms. Key as in Fig. 5.

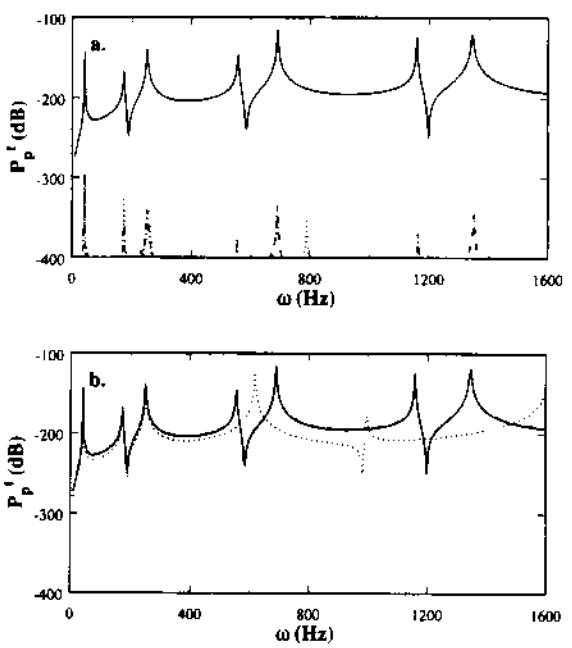

FIG. 8. Effect of truncation on normalized transmitted power through the force F_z path for the T-beam using approach C: (a) without correction terms, (b) with first-order correction terms. Key as in Fig. 5.

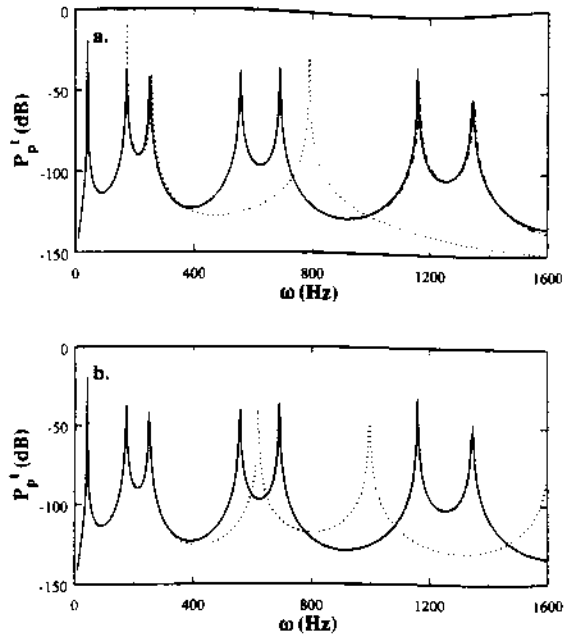

FIG. 9. Effect of truncation on normalized transmitted power through the moment M_z path for the T-beam using approach C: (a) without correction terms, (b) with first-order correction terms. Key as in Fig. 5.

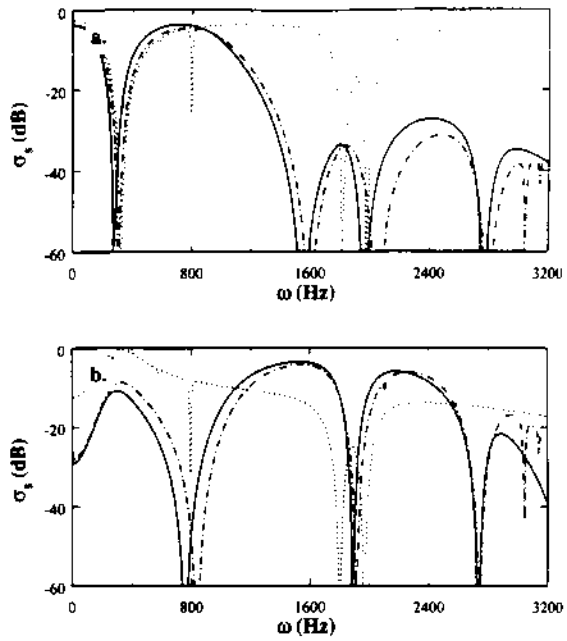

FIG. 11. Effect of truncation on modal dissipation efficiencies of receiver for the plate–beam structure using approach C. (a) Sixth plate mode, (b) eighth plate mode. Key: ——— n_z=460 (full), -·-· n_z=45, ··· n_z=25. Refer to Table I.

dent from the driving point accelerance and normalized input power spectra of Fig. 10. The signal-to-noise ratio problems of Fig. 3(b) are also seen here in Fig. 10(b). Over the frequency range of interest from 0 to 3200 Hz, five assembly modes are observed. For this example the following two cases are considered (again see Table I for details):

(i) Five (n_s) source CE or CL and ten (n_c) receiver CE or CL are retained which yields 25 (n_z) assembly modes, and

(ii) 15 (n_s) source CE or CL and 20 (n_c) receiver CE or CL are retained which yields 45 (n_z) assembly modes.

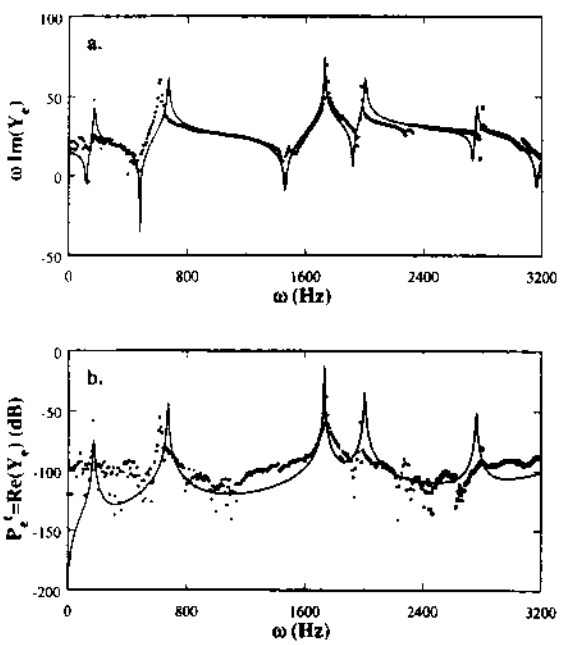

FIG. 10. Validation of power flow synthesis procedure for the plate–beam structure of Fig. 2(b). (a) Driving point accelerance, (b) normalized input power. Key: ——— theory, ··· experiment.

More modes were needed for this structure due to its higher dimension (i.e., it's a 3-D structure rather than 2-D like the T beam). For this structure, we will consider the effect of modal truncation upon the calculated modal dissipation efficiencies. In Fig. 11, the effect of the truncation upon the source efficiencies is shown. The first two elastic beam modes [in the x-z plane; Fig. 2(b)] are considered since they participate heavily in this frequency range. Note that now when we cite modes we are not referring to the CE or CL vectors. Rather we point to the modes of the transformed component mass and stiffness matrices which now correspond to the component UE basis with residual effects incorporated into it. It is these UE, $\mathbf{\Phi}_s$ and $\mathbf{\Phi}_c$, which are then used in the modal and mobility approaches. For both cases, n_z=45 and n_z=25, there is considerable discrepancy beyond 800 Hz, particularly for the n_z=25 case. However, the n_z=45 case does correctly capture the trends of the benchmark response. Note that the n_z=25 case incorrectly predicts that the first beam mode dissipates more efficiently at higher frequencies than the second beam mode. This is due to the insufficient basis of the n_z=25 case, and consequently the power or energy of the higher (truncated) modes are shifted onto the lower modes. Figure 12 shows the effect for the sixth and eighth elastic modes of the plate. Again these modes are chosen because they exhibit high participation in the frequency range of interest. It turns out that the sixth plate mode is about the highest mode which the n_z=25 case can predict and thus there is no n_z=25 case response for the eighth mode in Fig. 12(b). The n_z=45 case again correctly

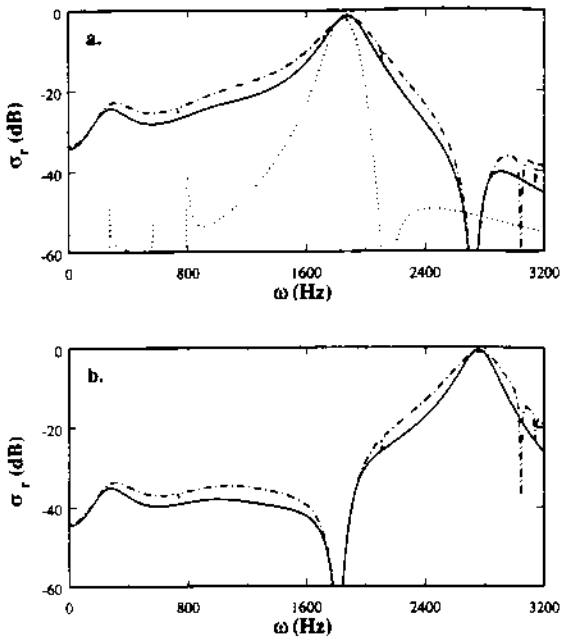

FIG. 12. Effect of truncation on modal dissipation efficiencies of source for the plate–beam structure using approach C. (a) First beam mode, (b) second beam mode. Key as in Fig. 11.

captures the trend of the benchmark responses in Fig. 12. Figure 13 shows the effect of the truncation on the power transmitted through the joint, for both the force and moment paths. As with the T-beam results, Figs. 8 and 9, responses for the force path seem more susceptible to the truncation. This is because the in-plane modes of the plate possess higher frequencies and therefore these are most likely to be truncated. Observe in Figs. 9 and 11–13 that the truncation

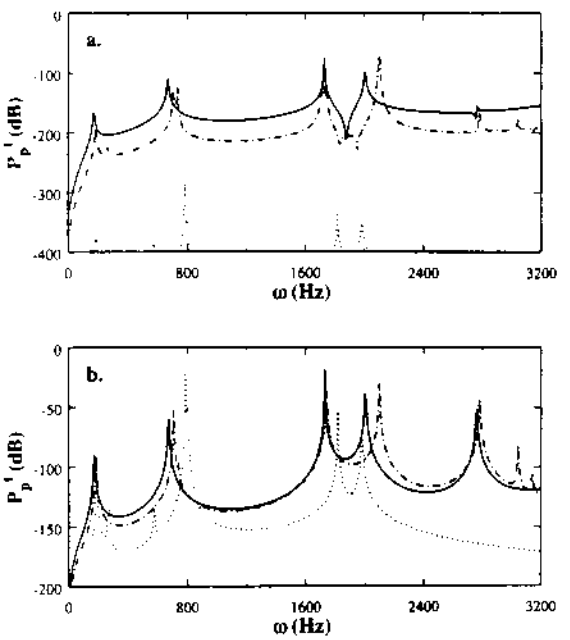

FIG. 13. Effect of truncation on normalized transmitted power for the plate–beam structure using approach C: (a) through the force F_y path, (b) through the moment M_x path. Key as in Fig. 11.

affects the transmitted power and modal dissipation efficiencies more than the input powers and accelerances.

VI. CONCLUSION

Three new approaches that minimize the effects of modal truncation in transmitted and dissipated vibratory power calculations have been proposed and comparatively evaluated. This methodology is particularly important for the successful implementation of power flow synthesis procedures[17,20] which are doubly susceptible to truncations in component modes. Each approach considers the components with constrained (fixed) boundary conditions at their interfaces, with their interior motion described by either eigenvectors (CE) or Lanczos vectors (CL). The choice of basis depends on the particular component. For instance, the use of CL on the source handles the localized response quite well. Similarly, the CE basis mimics the behavior of the receiver component in the absence of external loading. Such tailoring of the bases to each component has been found to be very beneficial. In fact, for the T-beam case considered, it relaxes the truncation criterion such that the number of retained basis vectors need only be about three times the number of modes of interest; for the plate–beam structure it is about nine times. The basis required in our studies is significantly less than that reported in previous studies[16,17] and thus sizable computational savings may be realized by approach C as proposed in this article. Future research will focus on the application of the proposed theory to more complicated structures and the means of integrating it into large scale computer codes. The effects of incorporating incomplete experimental databases of some components should be investigated.

ACKNOWLEDGMENT

This work has been supported by the U.S. Army Research Office (URI Grant No. DAAL-03-92-G-0120; Project Monitor: Dr. T. L. Doligalski).

[1] R. R. Craig, Jr., "A review of time-domain and frequency-domain component mode synthesis methods," Int. J. Anal. Exp. Modal Anal. **2**, 59–72 (1987).
[2] R. R. Craig, Jr., and A. L. Hale, "Block–Krylov component synthesis method for structural model reduction," J. Guid. Cont. **11**, 562–570 (1988).
[3] R. M. Hintz, "Analytical methods in component modal synthesis," AIAA J. **13** (8), 1007–1016 (1975).
[4] S. Rubin, "Improved component-mode representation for structural dynamic analysis," AIAA J. **13** (8), 995–1006 (1975).
[5] B. A. Brinkman, "A quantitative study using residual modes to improve dynamic models," Proceedings of the 5th IMAC, 1987, pp. 671–678.
[6] P. Leger and E. L. Wilson, "Modal summation methods for structural dynamic computations," Earthquake Eng. Struct. Dyn. **16**, 23–27 (1988).
[7] I. Hagiwara and Z. D. Ma, "Development of new mode-superposition technique for truncating lower- and/or higher-frequency modes (application to eigenmode sensitivity analysis)," JSME J., Ser. C **37** (1), 14–20 (1994).
[8] K. W. Min, T. Igusa, and J. D. Achenbach, "Frequency window method for forced vibration of multiply connected structural systems," J. Acoust. Soc. Am. **92**, 2726–2733 (1992).
[9] J. J. Allen, "A component synthesis method using Lanczos vectors," J. Modal Anal. **4**(2), 33–38 (1989).
[10] B. Nour-Omid and R. W. Clough, "Dynamic analysis of structures using Lanczos vectors," Earthquake Eng. Struct. Dyn. **12**, 565–577 (1984).

[11] E. L. Wilson, M. W. Yuan, and J. M. Dickens, "Dynamic analysis by direct superposition of Ritz vectors," Earthquake Eng. Struct. Dyn. **10**, 813–821 (1982).
[12] E. P. Bayo and E. L. Wilson, "Use of Ritz vectors in wave propagation and foundation response," Earthquake Eng. Struct. Dyn. **12**, 499–505 (1984).
[13] A. Curnier, "On three modal synthesis variants," J. Sound Vib. **90** (4), 527–540 (1983).
[14] O. Bernasconi and D. J. Ewins, "Modal strain/stress fields," J. Modal Anal. 4(2), 68–76 (1989).
[15] L. Gavric and G. Pavic, "A finite element method for computation of structural intensity by the normal mode approach," J. Sound Vib. **164** (1), 29–43 (1993).
[16] G. Pavic, "Energy flow induced by structural vibrations of elastic bodies," 3rd International Congress on Intensity Techniques, France, 1990, pp. 21–28.
[17] J. E. Farstad and R. Singh, "Effects of modal truncation errors on estimation of transmitted dynamic power estimates in discretely joined component assemblies," J. Acoust. Soc. Am. (accepted for publication).
[18] R. J. Guyan, "Reduction of stiffness and mass matrices," AIAA J. **3** (2), 380 (1965).
[19] ANSYS 5.0 User's Manual, Swanson Analysis Systems, 1992.
[20] T. E. Rook and R. Singh, "Power flow through multi-dimensional compliant joints using mobility and modal approaches," J. Acoust. Soc. Am. **97**, 1–10 (1995).
[21] J. F. Doyle, *Static and Dynamic Analysis of Structures* (Kluwer, Dordrecht, 1991).
[22] S. G. Braun and Y. M. Ram, "Predicting the effect of structural modification: upper and lower bounds due to modal truncation," J. Modal Anal. **6** (3), 201–213 (1991).
[23] D. A. Glasgow and H. D. Nelson, "Stability analysis of rotor-bearing systems using component mode synthesis," ASME J. Mech. Des. **102**, 352–359 (1980).
[24] D. F. Li and E. J. Gunter, "A study of the modal truncation error in the component mode analysis of a dual-rotor system," ASME J. Eng. Power **104**, 525–532 (1982).
[25] S. K. Tolani and R. D. Rocke, "Modal truncation of substructures used in free vibration analysis," ASME J. Eng. Ind. **98** (3), 827–834 (1976).
[26] P. Buchmann, J. M. Cushieri, and Y. Yong, "Structural power flow analysis using finite element," NOISE-CON, 1994, pp. 557–562.
[27] J. E. Farstad and R. Singh, "Analysis of transmitted vibration in a T-beam structure using component modes," NOISE-CON, 1994, pp. 579–584.
[28] B. A. T. Petersson, "A T-frame for analysis of structure-borne sound transmission by multi-point and component excitation," NOISE-CON, 1994, pp. 585–590.
[29] S. A. Hambric and A. J. Quezon, "Structure-borne noise predictions for a simple T-shaped beam," NOISE-CON, 1994, pp. 591–596.
[30] C. Burroughs, G. P. Carroll, and J. M. Cushieri, "Evaluation of structure-borne noise prediction techniques," NOISE-CON, 1994, pp. 541–544.
[31] R. S. Langley, "Analysis of power flow in beams and frameworks using the direct-dynamic stiffness method," J. Sound Vib. **136**, 439–452 (1990).
[32] G. Rosenhouse, H. Ertel, and F. P. Mechel, "Theoretical and experimental investigations of structure borne sound transmission through a T-joint in a finite system," J. Acoust. Soc. Am. **70**, 492–499 (1981).
[33] J. S. Przemieniecki, *Theory of Matrix Structural Analysis* (Dover, New York, 1968).
[34] T. C. Lim and R. Singh, "Vibration transmission through rolling element bearings. Part IV: statistical energy analysis," J. Sound Vib. **153** (1), 37–50 (1992).
[35] R. H. Lyon and T. D. Scharton, "Random vibration of connected structures," J. Acoust. Soc. Am. **36**, 1344–1354 (1964).
[36] M. M. Hrabok and T. M. Hrudey, "A review and catalogue of plate bending finite elements," Comp. Struct. **19** (3), 479–495 (1984).
[37] C. J. Camarada, R. T. Haftka, and M. F. Riley, "An evaluation of higher-order modal methods for calculating transient structural response," Comp. Struct. **27** (1), 89–101 (1987).
[38] L. E. Suarez and M. P. Singh, "Improved fixed interface method for modal synthesis," AIAA J. **30** (12), 2952–2958 (1992).
[39] G. O. Maldonado, M. P. Singh, and L. E. Suarez, "Random response of structures by a force derivative approach," J. Sound Vib. **155** (1), 13–29 (1992).